Raman backscattering saturation due to coupling between $_p$ and 2_p modes in plasma

2015 New J. Phys. 17 103026

(http://iopscience.iop.org/1367-2630/17/10/103026)

New Journal of Physics
The open access journal at the forefront of physics

Deutsche Physikalische Gesellschaft DPG
IOP Institute of Physics

Published in partnership with: Deutsche Physikalische Gesellschaft and the Institute of Physics

OPEN ACCESS

RECEIVED
9 April 2015

REVISED
9 September 2015

ACCEPTED FOR PUBLICATION
18 September 2015

PUBLISHED
14 October 2015

PAPER

Raman backscattering saturation due to coupling between ω_p and $2\omega_p$ modes in plasma

G Raj[1], B Ersfeld[1], G Vieux[1], S Yoffe[1], Min Sup Hur[2], R A Cairns[3] and D A Jaroszynski[1]

[1] Department of Physics, Scottish Universities Physics Alliance and University of Strathclyde, Glasgow G4 0NG, UK
[2] Department of Physics, UNIST, 50 Unist-gil, Ulju-gun, Ulsan, 689-798, Republic of Korea
[3] School of Mathematics and Statistics, University of St. Andrews, Fife KY16 9SS, UK

E-mail: d.a.jaroszynski@strath.ac.uk

Keywords: Raman amplification in plasma, saturation of parametric processes in plasma, plasma-based amplifiers

Abstract

Raman backscattering (RBS) in plasma is the basis of plasma-based amplifiers and is important in laser-driven fusion experiments. We show that saturation can arise from nonlinearities due to coupling between the fundamental and harmonic plasma wave modes for sufficiently intense pump and seed pulses. We present a time-dependent analysis that shows that plasma wave phase shifts reach a maximum close to wavebreaking. The study contributes to a new understanding of RBS saturation for counter-propagating laser pulses.

1. Introduction

Spatially homogeneous Raman backscattering (RBS) is the fastest growing of the Raman scattering instabilities that frequently occurs when a very long laser pulse propagates through plasma, such as in Raman amplification [1–5] and in laser driven inertial confinement fusion experiments, such as the National Ignition Facility (NIF) [6, 7] where it has a role in preheating the fuel pellet and degrading the implosion symmetry. In Raman amplification, a long (pump) laser pulse, with frequency ω_0 and wave number $\boldsymbol{k}_0$, is back scattered by a plasma wave (ω_p, $\boldsymbol{k}_p$) into a shorter counter-propagating (seed) laser pulse (ω_s, $\boldsymbol{k}_s$). The three waves need to satisfy the resonance conditions $\omega_s = \omega_0 - \omega_p$ and $\boldsymbol{k}_s = \boldsymbol{k}_0 - \boldsymbol{k}_p$, where $\omega_p = (e^2 n_0/m\varepsilon_0)^{1/2}$ with n_0 the plasma electron density, ε_0 the permittivity of free space and m and $-e$ being the electron rest mass and charge, respectively.

RBS growth and saturation has been extensively studied in the weakly coupled regime, at low pump laser intensities $a_0^2 \ll \omega_p/\omega_0 \ll 1$, where the growth rate is given by $\Gamma = a_0(\omega_0\omega_p)^{1/2}/2$ [8], and $a_0^2 \simeq 7.32 \times 10^{-19}\lambda_0(\mu\,\mathrm{m})I_0(\mathrm{W\,cm^{-2}})$ is the normalized intensity, λ_0 the laser wavelength and I_0 the intensity. For high pump intensities, $a_0^2 > 2\omega_p/\omega_0$, the three waves are strongly coupled and $\Gamma = \sqrt{3}\,\omega_p[\omega_0/(16\omega_p)]^{1/3}a_0^{2/3}$ [1]. A well defined growth rate in the linear regime has enabled theoretical [9–16] and experimental [17–19] progress in understanding the RBS saturation mechanism, especially in the nonlinear regime. Previous studies have shown that RBS can saturate via competing physical processes such as wavebreaking [9, 20–22], pump depletion [23] and relativistic mass change of plasma electrons [10, 12–14, 24] in both the linear and nonlinear regimes.

Nonlinear Raman amplification has been demonstrated experimentally e.g. seed pulses have been amplified to $\approx 2 \times 10^{13}$ W cm^{-2} (from an initial intensity $I_0 \approx 6 \times 10^{11}$ W cm^{-2}) and $\approx 1.3 \times 10^{16}$ W cm^{-2} ($I_0 \approx 1.3 \times 10^{12}$ W cm^{-2}) by pump lasers with intensities 9×10^{12} W cm^{-2} and 2×10^{14} W cm^{-2} respectively [2, 25, 26], for plasma densities $1 \times 10^{19} \leqslant n_0 \leqslant 3 \times 10^{20}$ cm^{-3}. In these experiments, amplification and pump depletion are accompanied by seed pulse compression, which leads to high intensities and an increased waveform steepness due to the high oscillation amplitude of the plasma wave. Nonlinear plasma-wave theory predicts that steepened plasma density perturbations include harmonics with amplitudes that increase relative to the fundamental plasma wave [27–29]. An early experiment provided evidence of plasma wave harmonic modes [30]. Moreover, a numerical study of nonlinear plasma waves has shown that second

harmonic plasma waves strongly influence the time evolution of the fundamental through a resonant wave–wave interaction [31].

In this paper, we investigate nonlinear growth and saturation of RBS in a parameter regime characterized by high density, cold, homogeneous and underdense plasma with intense initial seed and pump laser pulses. Parameters have been chosen to: (i) allow the seed to quickly enter the nonlinear pump depletion regime; (ii) ensure rapid saturation of nonlinear RBS to avoid development of Raman forward, modulational and filamenation instabilities; (iii) set a high wave breaking limit for the slow plasma wave (responsible for RBS, where $v_p \approx c\omega_p/2\omega_0 \ll c$), which has a significantly lower wave breaking limit compared with the fast plasma wave ($v_p \approx c$); and (iv) avoid Landau damping, which is higher in low density, warm plasma [32]. In this regime, beating between the pump and seed pulse drives large amplitude plasma waves that include harmonic modes [30, 33]. We show, for the first time, how coupling between the ω_p and $2\omega_p$ plasma wave modes feed back into the ω_p mode, leading to a plasma wave phase shift. This phase shift then competes with pump depletion and wavebreaking as mechanisms of RBS saturation. It should be noted that the present work is different from the study of the four-wave instability in [34], where coupling between slow and fast plasma waves is considered for two counter-propagating laser pulses with $\Delta\omega = \omega_0 - \omega_s = 2\omega_p$, which does not allow $2\omega_p$ modes to be produced.

We first present a theoretical model taking only the time-dependence into account, to identify and analyze the origin of the plasma wave phase shift. The structure of this paper is as follows: In section 2, a theoretical model to investigate coupling between fundamental and harmonic plasma wave modes is presented. Section 3 uses a 1D averaged particle-in-cell (PIC) code (*aPIC*) and a numerical analysis to study the nonlinearity arising from coupling between ω_p and $2\omega_p$ plasma wave modes. We also show the interplay between wavebreaking, pump depletion and the nonlinearity due to coupling between ω_p and $2\omega_p$ plasma wave modes at saturation. Conclusions are presented in section 4.

2. Theoretical model

Consider the electric fields of the pump, seed and plasma waves propagating through the plasma, to be given by $\boldsymbol{E}_j(\boldsymbol{r}, t) = (\hat{e}_j/2)[E_j \exp i(\boldsymbol{k}_j \cdot \boldsymbol{r} - \omega_j t) + \text{c.c.}]$, where $j = 0$, s, p represents the pump, seed and plasma waves, respectively, and $\boldsymbol{k}_j$, ω_j, $\hat{e}_j$ and E_j are the propagation vector, frequency, polarization vector and the slowly varying amplitude of the three waves. The wave equation in plasma is

$$\partial_t^2 \boldsymbol{E}(\boldsymbol{r}, t) + c^2 \nabla \times \nabla \times \boldsymbol{E}(\boldsymbol{r}, t) = -4\pi \partial_t \boldsymbol{J}(\boldsymbol{r}, t), \tag{1}$$

where $\boldsymbol{E}(\boldsymbol{r}, t)(=\boldsymbol{E}_0 + \boldsymbol{E}_s + \boldsymbol{E}_p)$ is the total electric field vector, with the individual fields satisfying $\nabla \cdot \boldsymbol{E}_0 = \nabla \cdot \boldsymbol{E}_s = 0$ and $\nabla \times \boldsymbol{E}_p = 0$, and $\boldsymbol{J} = -ne\boldsymbol{v}$ is the plasma current carried by the electrons moving with velocity $\boldsymbol{v}(\boldsymbol{r}, t)(=\boldsymbol{v}_0 + \boldsymbol{v}_s + \boldsymbol{v}_p)$. The cold relativistic fluid equations are given by $\partial_t \boldsymbol{v} = -e\boldsymbol{E}/m\gamma - e(\boldsymbol{v} \times \boldsymbol{B})/mc\gamma - (\boldsymbol{v} \cdot \nabla)\boldsymbol{v} - (\boldsymbol{v}/\gamma)(d_t\gamma)$ and $\partial_t(n_0 + \delta n) + \nabla \cdot [(n_0 + \delta n)\boldsymbol{v}] = 0$, where $\boldsymbol{B}(= \boldsymbol{B}_0 + \boldsymbol{B}_s)$ is the laser magnetic field vector with $\boldsymbol{B}_{0,s} = c(\boldsymbol{k}_{0,s} \times \boldsymbol{E}_{0,s})/\omega_{0,s}$, δn is the perturbed plasma density and $\gamma \approx (1 - \boldsymbol{v}^2/2c^2)^{-1}$ is the relativistic factor. Using the cold relativistic fluid equations, the rhs of equation (1) to third order in the fields is

$$\begin{aligned}\partial_t \boldsymbol{J} = en[&e\boldsymbol{E}/m + \nabla|\boldsymbol{v}|^2/2 - e\boldsymbol{v}(\boldsymbol{E} \cdot \boldsymbol{v})/mc^2 \\ &- E|\boldsymbol{v}|^2/2mc^2 + \boldsymbol{v}(\nabla \cdot \boldsymbol{v})] + e\boldsymbol{v}(\boldsymbol{v} \cdot \nabla\delta n).\end{aligned} \tag{2}$$

Equation (2) gives the linear and nonlinear current densities due to the three waves. Since the velocities of the plasma electrons under the influence of electric fields $\boldsymbol{E}_j$ is $\boldsymbol{v}_j(\boldsymbol{r}, t) = (e\hat{e}_j/2\ m\omega_j)$ $[-iE_j \exp i(\boldsymbol{k}_j \cdot \boldsymbol{r} - \omega_j t) + \text{c.c.}]$, for linearly polarized pump and seed, assuming that the plasma density perturbations obey Poisson's equation ($\delta n = -\nabla \cdot \boldsymbol{E}_p/4\pi e$), we can substitute equation (2) into equation (1), to obtain the time dependent [10, 12, 34] nonlinear mode-coupled equations for the slowly varying amplitudes E_j as

$$\partial_t E_l = -\chi_l \hat{E}_l + i\frac{\eta}{2}\kappa_l \left[\sum_{j=0,s,p} \Omega_{jl} E_j E_j^*\right] E_l,$$

$$\chi_l = \begin{cases} A[1 + \kappa_p/\kappa_s], \\ A[1 - \kappa_p], \\ -A, \end{cases} \quad \hat{E}_l = \begin{cases} E_s E_p, \\ E_0 E_p^*, \\ E_0 E_s^*, \end{cases}$$

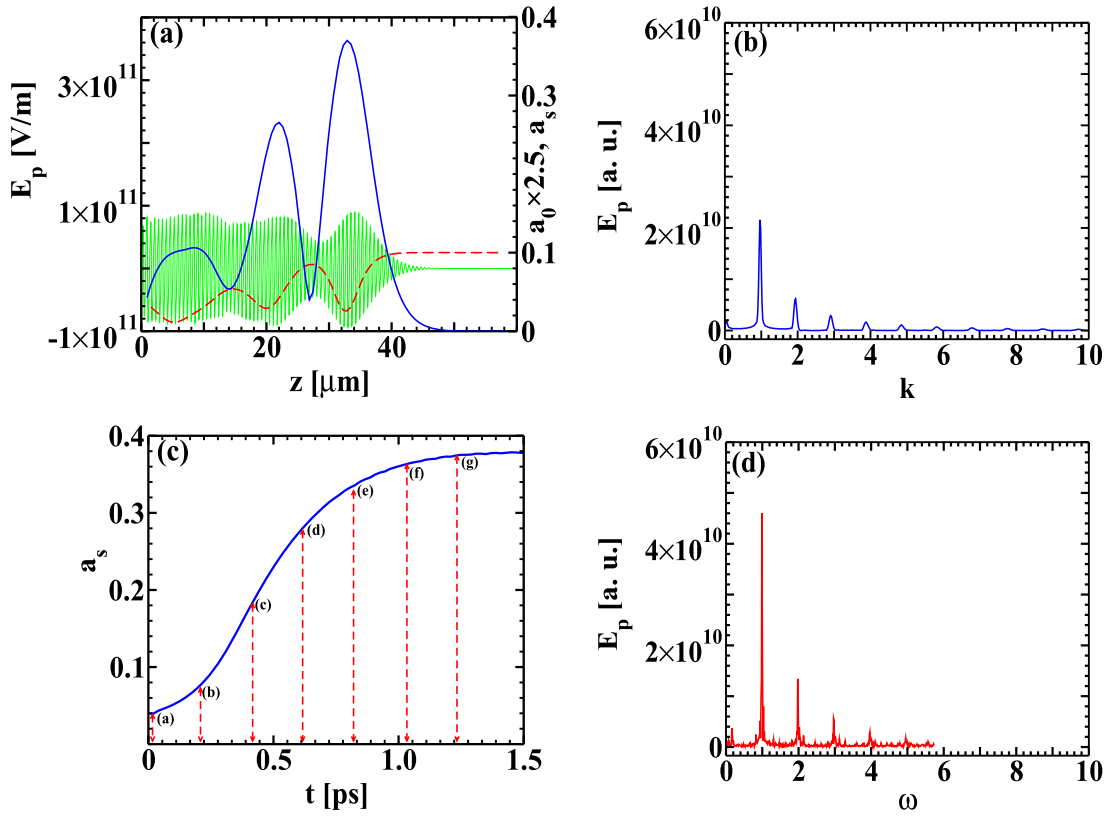

Figure 1. (a) A snapshot from simulations showing the evolution of the seed (blue curve), pump (red curve) and plasma wave (green curve) for $a_0 = a_s = 0.04$, $\omega_0 = 1.8\times10^{15}$ rad^{-1}, $\omega_s = 1.35 \times 10_{15}$ rad^{-1} and $\omega_0/\omega_p = 4$. (b) The spatial Fourier transform of E_p of the seed leading edge region (30–50 μm) in figure 1(a), normalized (by v_p/ω_p), as a function of the harmonic plasma wave number h_k, (c) variation of the seed leading edge peak a_s with time for the entire simulation with point (g) showing the time at which snapshot in figure 1(a) was taken; (d) temporal Fourier transform of E_p for the interval between points (f) and (g) in figure 1(a), as a function of the harmonic frequency h_ω normalized to ω_p.

$$\kappa_l = \begin{cases} 1, \\ \omega_0/\omega_s, \\ \omega_0/\omega_p, \end{cases} \qquad \Omega_{0l} = \begin{cases} 1/\kappa_s^2, & l = 0, \\ 4/3\kappa_s^2, & \text{for } l = \text{s}, \\ 2/3\kappa_s^2, & l = \text{p}, \end{cases}$$

$$\Omega_{pl} = \begin{cases} 2\kappa_p^2/3\kappa_s^2, \\ 2\kappa_p^2/3\kappa_s^2, \\ \rho\kappa_p^2/\kappa_s^2, \end{cases} \qquad \Omega_{sl} = \begin{cases} 2, \\ 1, \\ 2/3, \end{cases} \tag{3}$$

where $A = ek_p\omega_p/4\, m\omega_0\omega_s$, $\xi = e/2mc$, $\eta = 3A\xi\omega_p/ck_p\omega_s$ and $\rho = 1 - (8c^2k_0^2/\omega_p^2)$. In the nonlinear source ($\propto E_j^3$) on the rhs of the set of equations (3), the terms $\propto {E_p}^3$ are obtained from $e\boldsymbol{v}_p(\boldsymbol{v}_p \cdot \nabla\delta n)$ in the last term on the rhs of equation (2), and account for mode coupling between $2\omega_p$ (arising from $\boldsymbol{v}_p \cdot \nabla\delta n$) and ω_p plasma wave modes, while the remaining terms are due to relativistic effects. For electric field amplitudes of the form $E_j(t) = \varepsilon_j(t)\exp(\text{i}\alpha_j(t))$, where ε_j and α_j are the real amplitudes and phases respectively, the set of equations (3) describes the nonlinear coupled time dependent evolution of amplitudes and phases of the three waves, including mode coupling and relativistic effects, but disregarding any propagation effects.

3. Numerical and simulation results

To demonstrate how the presence of plasma wave harmonics leads to mode coupling nonlinearities as predicted by the set of equations (3), we first present 1D simulations using the code *aPIC* [35], where an infinitely long pump beam interacts with a short duration counter-propagating Gaussian seed pulse with full width at half maximum (FWHM) duration of 20 fs. It should be noted that the initial short seed pulse will broaden as it gets Raman amplified [1, 3, 5], leading to seed FWHM durations significantly larger than the plasma wave period. This ensures the applicability of the three wave coupling model in the given parameter regime, as long as the comparison with the simulations is restricted to the leading edge region (LER) of the probe, since propagation effects are not included in the model. Figure 1(a) presents a snapshot from the simulation showing resonant interaction between

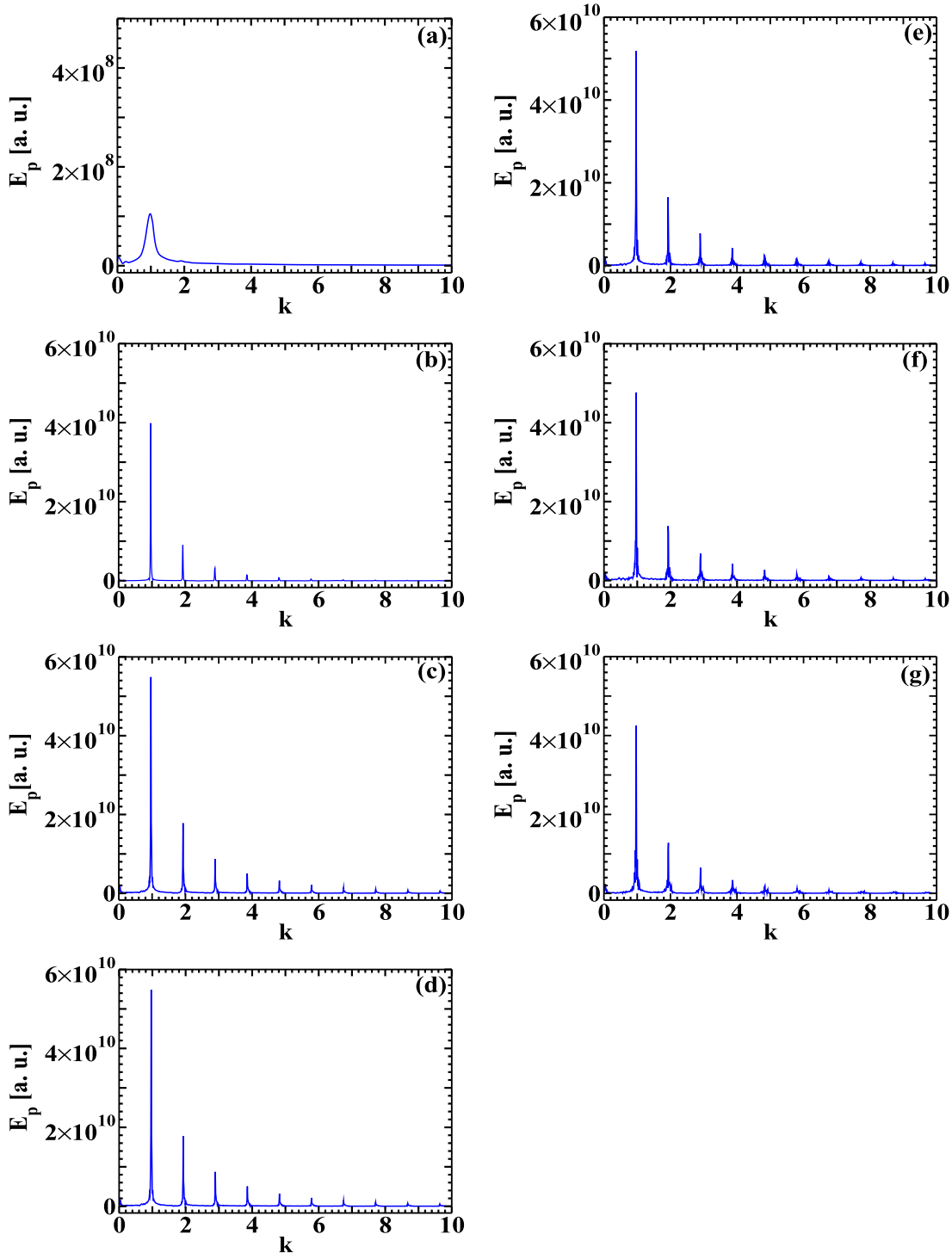

Figure 2. (a)–(g) Spatial Fourier transforms of E_p in the entire moving window region in snapshots (corresponding to points (a)–(g) in figure 1(c)) from simulation in figure 1. The figures show the change in magnitude of normalized (by v_p/ω_p) harmonic plasma wave numbers h_k with time.

the pump (dashed-red curve) and seed (solid-blue curve) pulses along with the generated plasma wave (solid-green curve). Figure 1(b) shows the Fourier transform of E_p in the seed LER extending from front (right edge) of the simulation window to the location of the seed leading edge peak a_s in figure 1(a). The plasma wave harmonic modes are clearly evident in the LER of the seed where there is resonant interaction between the three waves. Furthermore, in order to demonstrate the existence of plasma wave oscillations at $2\omega_p$, we also present the temporal Fourier transform (for the interval between points (f) and (g) in figure 1(c)) of E_p in figure 1(d). The figure clearly shows plasma wave oscillations at harmonic frequencies. Existence of the plasma wave harmonic modes has been demonstrated in early experiments by Umstadter *et al* [30]. Figure 1(c) shows the variation of the seed leading edge, peak a_s with time, where the point (g) shows the time at which figures 1(a) and 1(b) are obtained.

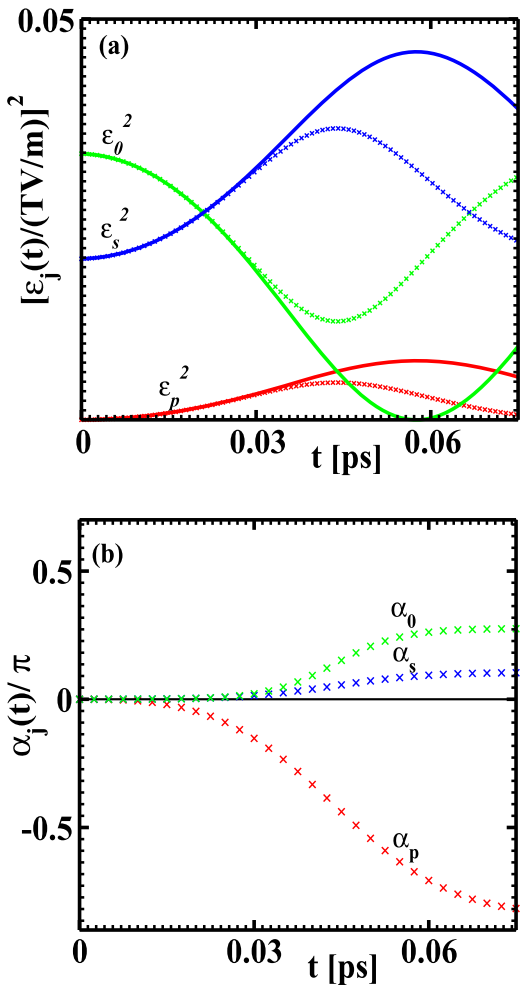

Figure 3. Evolution of (a) amplitudes and (b) phases with (crosses) and without (solid curves) plasma wave mode coupling and relativistic nonlinearities, for $a_0 = a_s = 0.04$, $\omega_0 = 1.8\times10^{15}$ rad^{-1}, $\omega_s = 1.35\times10^{15}$ rad^{-1} and $\omega_0/\omega_p = 4$.

The set of figures 2(a)–(g) show the evolution of the fundamental and harmonic plasma wave modes corresponding to figure 1. The figures show that during the initial stage (figure 2(a)) of interaction only the fundamental plasma wave mode is observed. However, as the plasma wave grows in amplitude with time (along with the seed in figure 1(c)), the harmonics of plasma wave appear (figure 2(b)) and increase in magnitude along with the fundamental till they become almost constant close to saturation (figure 1(c)) and then decrease. Also, it can be observed from the figures 1(b) and 2(g) that the restricted window for the Fourier transform of the seed LER region (figure 1(b)) leads to lower magnitude fundamental and harmonic plasma wave modes compared with the case where the entire moving window is used (figure 2(g)). Numerical solutions of equations (3), for the parameters used in the simulations, are presented in figure 3. The initial amplitudes and phases in figure 3 are, respectively, $\varepsilon_{00} = a_0 mc\omega_0/e$, $\varepsilon_{s0} = a_s mc\omega_s/e$, $\varepsilon_{p0} = 0.01\varepsilon_{00}$ and $\alpha_{00} = \alpha_{s0} = \alpha_{p0} = 0$. Figure 3(a) illustrates how the seed and plasma wave amplitudes grow to saturation, while satisfying the Manley–Rowe relations. The possible mechanisms of saturation in the regime explored are the nonlinear phase shift of the plasma wave due to coupling between ω_p and $2\omega_p$ modes, wavebreaking and pump depletion (loss of energy from pump to seed). Wavebreaking is defined as 'the loss of periodicity in at least one of the macroscopically observable quantities', such as the plasma wave electric field amplitude E_p. In terms of particle trapping, this occurs when a significant population of background plasma electrons are trapped [20]. Since the set of equation (3) cannot describe wavebreaking, we have used 1D *aPIC* simulations to verify this.

For the cold plasma used in the simulation (figure 1) and the theoretical analysis (figure 3), the wavebreaking limit is $E_{pmax} = (mc\omega_p/e)[2(\gamma_p - 1)]^{1/2} \approx 115$ GV m^{-1}, where $\gamma_p = [1 - (v_p/c)^2]^{-1/2}$ is the Lorentz factor relating to the phase velocity of the plasma wave [22]. Figure 1(a) shows that the peak plasma wave amplitude (green curve) of the seed LER is ≈88 GV m^{-1}, which is consistent with the theoretical predictions of 80 and 90 GV m^{-1} in the presence and absence of the nonlinearities, respectively, at saturation in figure 3(a). As these values are significantly lower than the wavebreaking limit, for the two cases presented in figure 3, wavebreaking

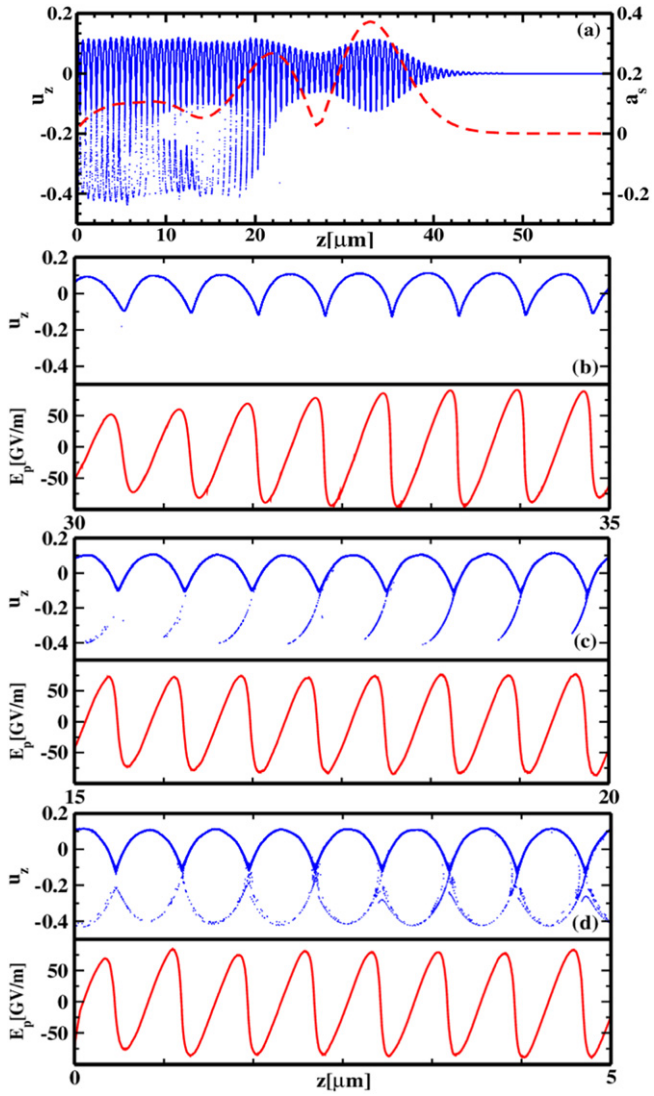

Figure 4. (a) Dotted-blue and dashed-red curves respectively showing normalized longitudinal velocity (u_z) of plasma electrons in phase space and the location of seed pulse in the moving window corresponding to simulations presented in figure 1. (b) shows u_z (blue-dotted curve) and E_p (solid-red curve) in the leading edge, while (c) and (d) show the same in the mid and tail regions, respectively.

can be ruled out as a mechanism for saturation. This is clear in the phase space analysis of plasma electrons presented in figure 4, at the same time step as figure 1(a). The blue-dotted curves in the figure show that in the seed LER (figure 4(a)) there is no particle trapping. However, in the mid (figure 4(b)) and tail (figure 4(c)) sections of the phase space, background plasma electrons are trapped by the plasma wave, and their number increases from the seed pulse leading edge to the tail region. For the given plasma density and approximately an order of magnitude lower pump and seed intensities (non-relativistic) 1D PIC simulations presented in [36] show similar trapping for thermal plasma with a temperature of ≈50 eV. The solid-red curves show that, although a small fraction of background plasma electrons are trapped, the corresponding collective plasma electron oscillations (leading to E_p) preserve their periodicity in the three regions, thus clearly proving that wavebreaking does not occur. Figure 3(a) shows that in presence of nonlinearities due to coupling between ω_p and $2\omega_p$ plasma wave modes and relativistic effects (crosses), RBS saturates at early times compared with the case where nonlinearities are neglected (solid curves).

Figure 3(b) shows that there is a significant shift in the plasma wave phase α_p due to the mode coupling nonlinearities during saturation, whereas without them the wave phases do not change (solid-black curve). Figure 3(a) shows that switching off the mode coupling and relativistic nonlinearities leads to complete pump depletion (solid-green curve), which is reduced to ≈65% (cross-green curve) when the nonlinearities are included. This leads to a reduction of the maximum seed and plasma wave amplitudes by 20% and 35% when nonlinearities are present, compared with the case where they are absent. This is due to the plasma wave phase shift, which detunes the resonant three wave system and reduces backscattering of the pump (lower pump

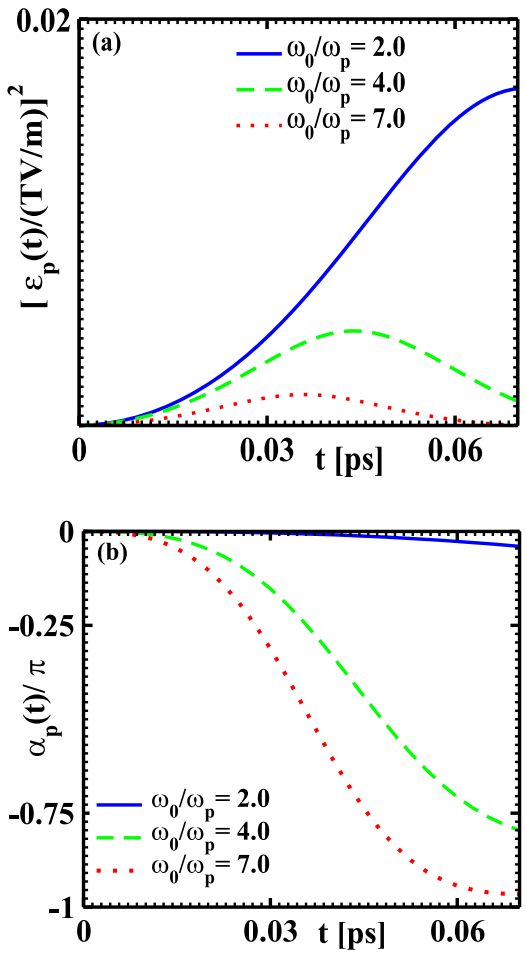

Figure 5. Temporal evolution of (a) amplitudes and (b) phases of the plasma wave in presence of mode coupling and relativistic nonlinearities with variation in plasma density for $a_0 = a_s = 0.04$ and $\omega_0 = 1.8\times10^{15}$ rad^{-1}.

depletion) into the seed, while in the absence of the nonlinearities the system is perfectly tuned and leads to complete pump depletion. Further, as will be shown later, among the two nonlinearities, relativistic effects are not significant for these cases. An important new observation in the present regime is that the saturation time is significantly smaller than observed in previous studies [10, 12, 24] that included a noise source a_s and considerably higher a_0. This can be explained, in the present regime, because the initial seed is sufficiently intense, even for low pump a_0 (compared with the previous studies) the ponderomotive beat between a_0 and a_s is strong, which drives a large amplitude plasma wave with $2\omega_p$ mode that couples with ω_p mode causing the plasma wave phase shift, which saturates RBS at an earlier time. It should be noted that in the present case, for amplified seed a_s and a_0 smaller than in the previous studies, relativistic effects are weak (as shown below). For the case of RBS seeded by noise, even though a_0 is large the ponderomotive beat is weak until the time when the seed is significantly amplified (which delays saturation). However, when a_s has been amplified significantly, because of the higher a_0 (compared with the current regime) relativistic effects become important in causing the phase shift. Also, recent studies [13, 14] have shown that for pump intensities much lower than that used in the present and previous [10, 12, 24] studies, the seed can be amplified to ultra-high intensity ($\approx10^{18}$ W cm^{-2}), which is an order of magnitude higher leading to saturation due to relativistic effects.

Figures 5(a) and (b), respectively, show the evolution of the plasma wave amplitude and phase (from equation (3)) for different plasma densities (all other parameters are the same as those used for figure 1) in the presence of mode coupling and relativistic nonlinearities. The figures show that for dense plasma ($\omega_0/\omega_p = 2.0$), where the wavebreaking limit is high, and for the same initial pump and seed amplitudes, the plasma wave phase shift (figure 5(b)) is reduced thus taking a longer time to saturate. This allows the plasma wave to grow to a large amplitude (figure 5(a) solid curve) before saturation. Lowering the plasma density ($\omega_0/\omega_p = 4$ and 7) leads to an enhanced plasma wave phase shift, which causes saturation at an earlier time, leading to lower amplitude plasma waves. However, for the $\omega_0/\omega_p = 7$, figure 5(a) shows that the plasma wave amplitude at saturation is 37 GV m^{-1}, which exceeds the wavebreaking limit of 34 GV m^{-1}. Wavebreaking is therefore the main

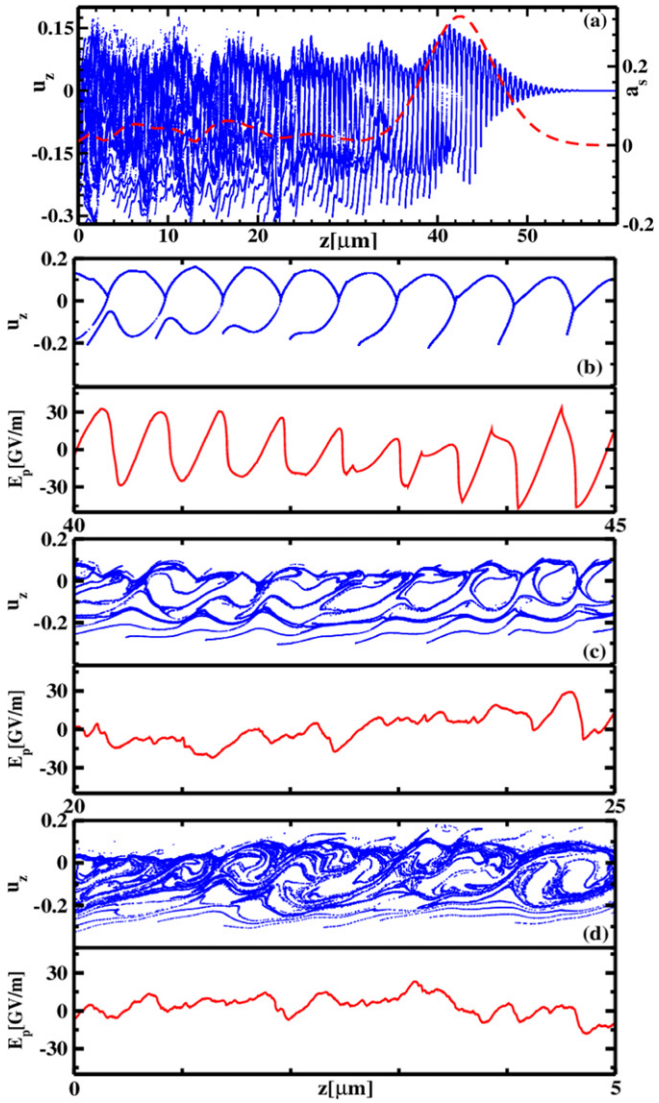

Figure 6. (a) Dotted-blue and dashed-red curves respectively showing normalized longitudinal velocity (u_z) of plasma electrons in phase space and location of seed pulse in the moving window of 1 d *aPIC* simulations for $\omega_0/\omega_p = 7$ case with other parameters same as used in figure 1. Starting from the right edge (b) shows u_z (blue-dotted curve) and E_p (solid-red curve) in the leading edge, while (c) and (d) show the same in the mid and tail regions, respectively.

mechanism of saturation, which occurs more quickly compared to saturation due to the plasma wave phase shift [9]. This can be verified from figure 6, where the dotted-blue and dashed-red curves in figure 6(a) show, respectively, the electron phase space for $\omega_0/\omega_p = 7$ and the location of seed pulse in the simulation box. It is observed from the dotted-blue curves in the figure, that a significant fraction of background plasma electrons are trapped in the seed LER region (figure 6(b)), and significantly enhanced in the mid (figure 6(c)) region, while almost all plasma electrons are trapped in the tail (figure 6(d)). The corresponding solid-red curves in the figures show that moving from the leading edge towards the tail region, increased plasma electron trapping leads to disruption of the periodicity in the collective plasma electron oscillations (observed as E_p), which eventually collapses and loses its structure in the tail region, which confirms the presence of wavebreaking. It should be noted that in such a strong particle trapping regime frequency shifts due to trapped particles [37] can also become important for non-relativistic seed and pump in warm plasmas and it can increase with the increase in temperature [36]. In figure 7 plasma wave phase evolution is plotted with (dashed-red curve) and without (solid curve) relativistic effects (using equation (3)), for $a_0 = a_s = 0.08$ (blue curves) and 0.04 (green curves). The figure shows that the mode coupling nonlinearity is the dominant physical process leading to a shift in the plasma wave phase in this parameter regime, where the pump and seed intensities are low and relativistic effects [10, 12, 24] (dashed curves) only mildly reduce the plasma wave phase shift (by 6.6% and 7.3% respectively for $a_0 = a_s = 0.08$ and 0.04).

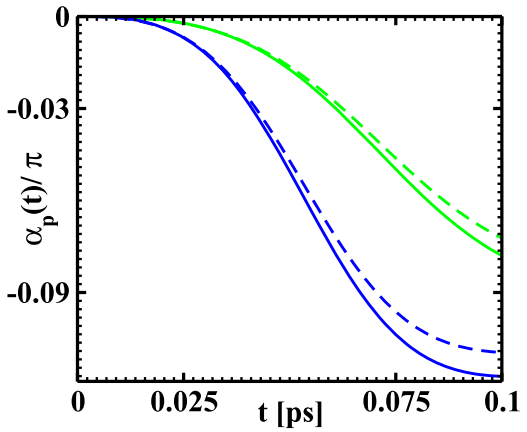

Figure 7. Plasma wave phase evolution in presence (dashed curve) and in absence (solid curve) of the relativistic effects for $a_0 = a_s = 0.08$ (blue curves) and 0.04 (green curves), for $\omega_0 = 1.8 \times 10^{15}$ rad^{-1}, and $\omega_0/\omega_p = 2$.

4. Conclusions

In this paper, using 1D simulations for the laser-plasma parameters relevant to Raman amplifiers operating in the nonlinear RBS regime [2, 26], we show the existence of plasma wave harmonic modes in the LER of the seed pulse. Using a three wave model and a time-dependent analysis we identify a new physical process i.e. coupling between the fundamental ω_p and harmonic $2\omega_p$ plasma wave modes, which can contribute to the nonlinear source driving the three resonant waves in RBS via higher order interactions. Such a nonlinearity is shown to excite a plasma wave phase shift that detunes the resonant three wave RBS process, leading to its saturation. In the regime of interest, the plasma wave phase shift due to coupling between the ω_p and $2\omega_p$ plasma wave modes is shown to dominate other physical processes such as wavebreaking, relativistic effects and pump depletion in saturation. The study shows that for sufficiently intense laser pulses and dense plasma, the nonlinearity arising from coupling between the ω_p and $2\omega_p$ modes can saturate RBS before the occurrence of wavebreaking. However, in the case of low density plasmas, as was also shown in earlier studies [9], wavebreaking dominates as the saturation mechanism. An important observation is that in the current regime with sufficiently intense seed and pump pulses, the nonlinear phase shift is caused primarily due to coupling between ω_p and $2\omega_p$ modes, and relativistic effects only mildly affect the phase shift. The study shows that RBS saturates at an earlier time compared with previous regimes (using noise as a seed, and significantly higher pump intensity) [10, 12, 24] where the saturation time is longer and the relativistic effects play an important role.

Furthermore, in the present case (with $\Delta\omega = \omega_p$) the laser intensity threshold for the excitation of a fast plasma wave is significantly higher compared with the four-wave instability case (with $\Delta\omega = 2\omega_p$) [34]. As a consequence, no fast plasma waves are observed until saturation (this can be seen from the simulation results in figure 1) in the present regime of study. However, for Raman amplifiers operating in regimes where the seed becomes intense (due to amplification) and begins to drive a fast plasma wave, a small frequency shift due to coupling between slow and fast plasma waves is introduced, which we expect will add to the frequency shift due to coupling between the ω_p and $2\omega_p$ plasma wave modes and relativistic effects, which saturates RBS. Similar coupling between fundamental and harmonic ion acoustic waves could also play an important role in the rapidly emerging field of pulse amplification using strong-coupling stimulated Brillouin Scattering [38, 39], since it has been shown that harmonics of ion acoustic waves can be present during Brillouin scattering process [40].

Acknowledgments

We acknowledge the support of the UK EPSRC (grant no. EP/J018171/1), the EU FP7 programmes: the Extreme Light Infrastructure (ELI) project, the Laserlab-Europe (no. 284464), and the EUCARD-2 project (no. 312453), University of Strathclyde High Performance Computer (USE-HPC) facility. Results were obtained using the EPSRC funded ARCHIE-WeSt High Performance Computer (www.archie-west.ac.uk), EPSRC grant no. EP/K000586/1. The data associated with this research is available at doi: 10.15129/0d10d9a7-ced8-446c-a65d-09a1bc9e546d.

References

[1] Shvets G, Fisch N J, Pukhov A and Meyer-ter Vehn J 1998 *Phys. Rev. Lett.* **81** 4879
[2] Ren J, Cheng W, Li S and Suckewer S 2007 *Nat. Phys.* **3** 732
[3] Ersfeld B, Farmer J, Raj G and Jaroszynski D A 2010 *Phys. Plasmas* **17** 083301
[4] Hur M S, Hwang I, Jang H J and Suk H 2006 *Phys. Plasmas* **13** 073103
[5] Vieux G *et al* 2011 *New J. Phys.* **13** 065031
[6] Lindl J D and Moses E I 2011 *Phys. Plasmas* **18** 050901
[7] Kirkwood R K *et al* 2011 *Phys. Plasmas* **18** 056311
[8] Kruer W L 1988 *The Physics of Laser Plasma Interactions* (Reading, MA: Addison-Wesley)
[9] Malkin V M, Shvets G and Fisch N J 1999 *Phys. Rev. Lett.* **82** 4448
[10] Raj G, Upadhyaya A K, Mishra R K and Jha P 1997 *Phys. Lett.* A **371** 135
[11] Trines R M G M *et al* 2011 *Nat. Phys.* **7** 87
[12] Jha P, Raj G and Upadhyaya A K 2006 *IEEE Trans. Plasma Sci.* **34** 922
[13] Malkin V M, Toroker Z and Fisch N J 2014 *Phys. Plasmas* **21** 093112
[14] Malkin V M, Toroker Z and Fisch N J 2014 *Phys. Rev.* E **90** 063110
[15] Clark D S and Fisch N J 2003 *Phys. Plasmas* **10** 4848
[16] Toroker Z, Malkin V M and Fisch N J 2014 *Phys. Plasmas* **21** 113110
[17] Yampolsky N A and Fisch N J 2011 *Phys. Plasmas* **18** 056711
[18] Yampolsky N A, Fisch N J, Malkin V M, Valeo E J, Lindberg R, Wurtele J, Ren J, Li S, Morozov A and Suckewer S 2008 *Phys. Plasmas* **15** 113104
[19] Ren J, Li S, Morozov A, Suckewer S, Yampolsky N A, Malkin V M and Fisch N J 2008 *Phys. Plasmas* **15** 056702
[20] Bergmann A and Mulser P 1993 *Phys. Rev.* E **47** 3585
[21] Akhiezer A I and Polovin R V 1956 *Sov. Phys. JETP* **3** 696
[22] Mori W B and Katsouleas T 1990 *Phys. Scr.* T **30** 127
[23] Horton W and Tajima T 1986 *Phys. Rev.* A **34** 4110
[24] Miyakoshi T *et al* 2002 *Phys. Plasmas* **9** 3552
[25] Ping Y, Geltner I, Fisch N J, Shvets G and Suckewer S 2000 *Phys. Rev.* E **62** R4532
[26] Cheng W, Avitzour Y, Ping Y, Suckewer S, Fisch N J, Hur M S and Wurtele J S 2005 *Phys. Rev. Lett.* **94** 045003
[27] Dawson J M 1959 *Phys. Rev.* **113** 383
[28] Jackson E A 1960 *Phys. Fluids.* **3** 831
[29] Koch P and Albritton J 1975 *Phys. Rev. Lett.* **34** 1616
[30] Umstadter D, Williams R, Clayton C and Joshi C 1987 *Phys. Rev. Lett.* **59** 292
[31] Klozenberg J P 1971 *Phys. Fluids.* **14** 94
[32] Farmer J P, Ersfeld B and Jaroszynski D A 2010 *Phys. Plasmas* **17** 113301
[33] Everett M J, Lal A, Clayton C E, Mori W B, Johnston T W and Joshi C 1995 *Phys. Rev. Lett.* **74** 2236
[34] Shvets G and Fisch N J 2001 *Phys. Rev. Lett.* **86** 3328
[35] Hur M S, Penn G, Wurtele J S and Lindberg R 2004 *Phys. Plasmas* **11** 5204
[36] Wang T-L, Clark D S, Strozzi D J, Wilks S C, Martins S F and Kirkwood R K 2010 *Phys. Plasmas* **17** 023109
[37] Morales G J and O'Neil T M 1972 *Phys. Rev. Lett.* **28** 417
[38] Lancia L *et al* 2010 *Phys. Rev. Lett.* **104** 025001
[39] Guillaume E *et al* 2014 *High Power Laser Sci. Eng.* **2** 1
[40] Casanova M, Laval G, Pellat R and Pesme D 1972 *Phys. Rev. Lett.* **54** 2230